The Journal of Chemical Physics ARTICLE scitation.org/journal/jcp

Size-selected anion photoelectron spectroscopy and density functional theory study of $MnC_n^{-/0}$ (n = 3-10): Odd-even alternation and linear-cyclic structure competition

Cite as: J. Chem. Phys. 150, 074304 (2019); doi: 10.1063/1.5084310
Submitted: 6 December 2018 • Accepted: 30 January 2019 •
Published Online: 19 February 2019

Xi-Ling Xu,[1,2,a] Bin Yang,[1,2] Chao-Jiang Zhang,[1,2] Hong-Guang Xu,[1,2] and Wei-Jun Zheng[1,2,a]

AFFILIATIONS

[1] Beijing National Laboratory for Molecular Sciences (BNLMS), State Key Laboratory of Molecular Reaction Dynamics, Institute of Chemistry, Chinese Academy of Sciences, Beijing 100190, China
[2] University of Chinese Academy of Sciences, Beijing 100049, China

[a] **Authors to whom correspondence should be addressed:** xlxu@iccas.ac.cn and zhengwj@iccas.ac.cn, **Tel.:** +86 10 62635054, **Fax:** +86 10 62563167.

ABSTRACT

The structural and electronic properties of MnC_n^- (n = 3-10) clusters have been investigated using size-selected photoelectron spectroscopy and density functional theory calculations. The vertical detachment energies of MnC_n^- exhibit a strong odd-even alternation with increasing number of carbon atoms: the vertical detachment energies of MnC_n^- containing even number of carbon atoms are higher than those of adjacent ones containing odd number of carbon atoms. The theoretical analyses indicate that the spin multiplicities and relative stabilities of $MnC_n^{-/0}$ also exhibit odd-even alternations. It is found that MnC_3^- has three degenerate isomers with two linear structures in different electronic states and one fanlike structure. For n = 4-6, 8, and 10, the ground state structures are all linear with the Mn atom at one end. MnC_7^- and MnC_9^- have cyclic structures. As for the neutral species, MnC_3 and MnC_4 adopt fan-shaped structures, MnC_5 has a linear structure, and MnC_{6-10} have cyclic configurations. The atomic dipole moment corrected Hirshfeld population analysis shows that the electrons transfer from the Mn atom to the C_n units. The total spin magnetic moments of $MnC_n^{-/0}$ (n = 3-10) clusters are mainly contributed by the local magnetic moments on the Mn atom.

I. INTRODUCTION

The doping of carbon clusters with transition metals may induce unique physical and chemical properties and therefore have potential applications in the fields of catalysis and functional materials. It has been reported that transition metals and carbon not only can form metallocarbohedrenes (metcars)[1–4] and endohedral metallofullerenes[5,6] but also can form two-dimensional metal carbides such as MXenes, which may be used as electrode materials for batteries and supercapacitors.[7–9] Due to the special metal-carbon interactions, late transition metals such as Fe, Co, and Ni can act as catalysts in carbon nanotubes' growth.[10–13]

In the last decades, metal carbide clusters were investigated by experiment and theory intensively. Wang and co-workers investigated the structures and electronic properties of small MC_n^- (M = Fe, Ti, Cr, Nb)[14–18] clusters using anion photoelectron spectroscopy. Knappenberger *et al.* studied the structures of diniobium-carbon clusters using anion photoelectron spectroscopy and density functional theory (DFT) calculations.[19] Zheng and co-workers investigated the structural and electronic properties of $Co_mC_n^-$[20,21] and $V_mC_n^-$[22] using size-selected anion photoelectron spectroscopy in combination with DFT calculations. The structural properties of AuC_n^- clusters were explored by using a time-of-flight (TOF) mass spectrometer and DFT calculations.[23] The structure

of $Au_2C_2^-$ has been investigated with size-selected anion photoelectron spectroscopy,[24] and those of $Au(C{\equiv}C)_nAu^-$ (n = 1–3) were studied using a high-resolution photoelectron imaging technique.[25] It has been suggested that metal carbide clusters such as MoC_3^-, $Ta_2C_4^-$, and FeC_6^- have intriguing catalytic properties in the reactions involving C–H bond activation.[26–28] The theoretical studies of Redondo *et al.* suggested that the structures of 3d mono-metal carbides $TMC_n^{\pm/0}$ (TM = Sc, Ti, V, Fe, Co, and Zn; n = 1-8)[29–41] are related to the number of d electrons of the TM atom and the cluster sizes. The structural and electronic properties of the $(FeC)_n$ and $MC_n^{+/0}$ (M = Y, La) clusters were investigated using density functional theory calculations.[42,43] Recently, the structures and properties of $Pt_3C_2^{-/0}$ and $Pt_{1-7}C_2^{-/0}$ were also investigated with density functional theory.[44,45]

Manganese carbides are possible carbon-bearing molecules in stellar objects and interstellar media, especially in the carbon rich envelope of stars, because both carbon and manganese have relatively large cosmic abundances.[46] First-principles calculations suggested that $Mn_{23}C_6$ is one of the most stable phases among the binary carbides $M_{23}C_6$ (M = V–Ni).[47] Recent theoretical studies predicted Mn-based MXene (Mn_2CF_2) to be a half-metal with a wide half-metallic gap and room-temperature ferromagnetism, which has potential applications in spintronics.[48] Density functional theory calculations proposed Mn_2C sheets to be promising electrode materials for lithium-ion batteries.[49] There are only a few experimental and theoretical studies on small manganese carbide clusters. Borin and Gobbo conducted high level calculations on the low-lying quartet electronic states of diatomic MnC employing a multireference configuration interaction (MRCI) approach based on complete-active-space self-consistent-field (CASSCF) wave functions.[50] Gutsev *et al.* calculated the spectroscopic constants, electron affinities, ionization energies, and dissociation energies of diatomic $MnC^{\pm/0}$ based on density functional theory.[51] The vibrationally resolved spectra of MnC_2^- and MnC_3^- were studied by using anion photoelectron spectroscopy.[52,53] In order to help understand the geometrical structures and electronic properties of manganese carbide clusters and to provide useful information for future high resolution spectroscopy studies, in this work, we conducted a combined size-selected anion photoelectron spectroscopy and density functional theory study on $MnC_n^{-/0}$ (n = 3-10) clusters.

II. EXPERIMENTAL AND THEORETICAL METHODS

A. Experimental methods

The experiments were performed using a home-built apparatus consisting of a time-of-flight (TOF) mass spectrometer and a magnetic-bottle photoelectron spectrometer, which has been described previously.[54] Briefly, the MnC_n^- (n = 3–10) cluster anions were generated in a laser vaporization source by laser ablation of a rotating and translating manganese-carbon mixture disk target (13 mm diameter and Mn:C mole ratio 5:1) with the second harmonic light (532 nm) of a Nd:YAG laser (Continuum Surelite II-10), while helium gas with ~4 atm backing pressure was allowed to expand through a pulsed valve (General Valve Series 9) over the target for cooling the formed clusters. The cluster anions were mass-analyzed by using the TOF mass spectrometer. The MnC_n^- (n = 3–10) clusters were each mass-selected and decelerated before being photodetached using the fourth harmonic light (266 nm) of another Nd:YAG laser. The photodetached electrons were energy-analyzed by using the magnetic-bottle photoelectron spectrometer. The energy resolution of the photoelectron spectrometer was approximately 40 meV for the electrons of 1 eV kinetic energy. The photoelectron spectra were calibrated using the spectra of Cu^- and Au^- taken under similar conditions.

B. Theoretical methods

The structures of MnC_n^- (n = 3–10) clusters and their neutral counterparts were optimized using DFT with Becke's three-parameter and Lee-Yang-Parr's gradient-corrected correlation hybrid functional (B3LYP)[55,56] and 6-311+G(d) basis set as implemented in the Gaussian 09 program package.[57] To confirm the reliability of the 6-311+G(d) basis set, we also calculated the relative energies and vertical detachment energies (VDEs) of the MnC_{3-5}^- clusters at the B3LYP/aug-cc-pVTZ level. The results at the B3LYP/6-311+G(d) level are very close to those at the B3LYP/aug-cc-pVTZ level (see Table S1 in the supplementary material). Therefore we chose the 6-311+G(d) basis set for the larger MnC_n and MnC_n^- species. We have considered all possible spin multiplicities during the calculations. All the geometry optimizations were conducted without any symmetry constraint. Harmonic vibrational frequencies were calculated to make sure that the optimized structures correspond to true local minima. The zero-point vibrational energy corrections were included for the relative energies and adiabatic detachment energies (ADEs) of isomers. The theoretical VDE was calculated as the energy difference between the neutral and anion states at the geometry of the anionic species. The theoretical ADE was obtained as the energy difference between the neutral and anion states, with the neutral optimized to the nearest local minimum to the anionic geometry. The atomic dipole moment corrected Hirshfeld (ADCH) population analysis[58] of $MnC_n^{-/0}$ (n = 3–10) was performed with the Multiwfn program.[59] The ADCH charge analysis is an improved version of the Hirshfeld charge analysis.[60]

III. EXPERIMENTAL RESULTS

The photoelectron spectra of MnC_n^- (n = 3–10) taken with 266 nm (4.661 eV) photons are presented in Fig. 1. The VDEs and ADEs of these clusters estimated from their photoelectron spectra are listed in Table I. The VDE of each cluster was taken from the maximum of the first peak in its spectrum. The ADE of each cluster was determined by adding the value of instrumental resolution to the onset of the first peak in its spectrum. The onset of the first peak was determined by drawing a straight line along the

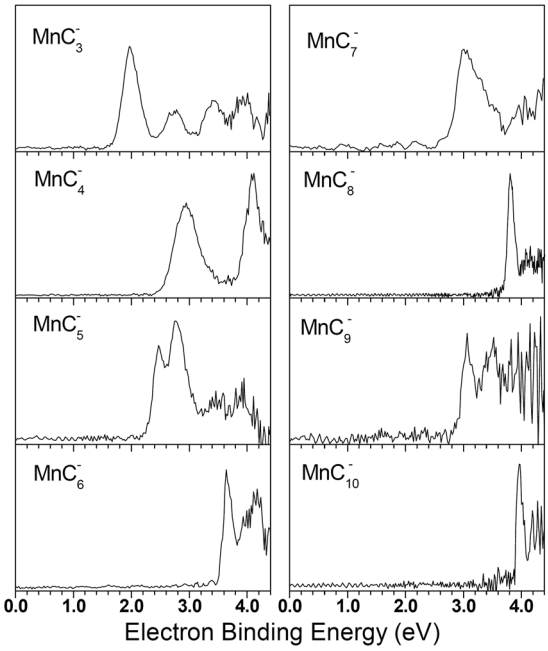

FIG. 1. Photoelectron spectra of MnC_n^- (n = 3–10) clusters recorded with 266 nm photons.

leading edge of the first peak to cross the baseline of the spectrum.

The photoelectron spectrum of MnC_3^- has five resolved peaks centered at 1.96, 2.74, 3.39, 3.93, and 4.17 eV, respectively. The spectrum of MnC_3^- had been measured at 532 nm by Wang and Li.[53] In this work, the spectrum recorded at 266 nm shows the higher binding energy peaks which cannot be accessed by 532 nm photons. There are two well-resolved peaks centered at 2.95 and 4.12 eV in the spectrum of MnC_4^-. The spectrum of MnC_5^- displays two peaks centered at 2.47 and 2.76 eV, followed by some undistinguishable features at the high binding energy side. As for the spectrum of MnC_6^-, there is a strong peak centered at 3.64 eV, followed by a broad feature centered at 4.11 eV. In the spectrum of MnC_7^-, there is a broad band centered at 3.01 eV with the shoulders of 3.29 and 3.56 eV, followed by some features at the high binding energy side. The spectrum of MnC_8^- has a strong peak centered at 3.81 eV, followed by some weak features at the high binding energy side. The spectrum of MnC_9^- shows two resolved peaks centered at 3.06 and 3.52 eV. The spectrum of MnC_{10}^- displays four peaks centered at 3.97, 4.19, 4.28, and 4.34 eV, respectively.

IV. THEORETICAL RESULTS AND DISCUSSION

The typical low-lying isomers of the MnC_n^- (n = 3-10) clusters obtained from DFT calculations are presented in Fig. 2 with the most stable ones on the left, and those of neutral MnC_n are displayed in Fig. 3. The relative energies, theoretical VDEs, and ADEs of these low-lying isomers are summarized in Table I, along with the experimental VDEs and ADEs for comparison. We also simulated the photoelectron spectra of the low-lying isomers of MnC_n^- (n = 3-10) based on the generalized Koopmans' theorem (GKT)[61,62] and compare the simulated spectra with the experimental spectra in Fig. 4. The simulated spectra are named as density of states (DOS) spectra for convenience. The simulated spectra were obtained by fitting the distributions of the transition lines with unit-area Gaussian functions of 0.2 eV full width at half maximum (FWHM).

Figure 5 shows a comparison of the theoretical VDEs of the most stable structures of MnC_n^- with the experimental values. Both the experimental and theoretical results demonstrate that the VDEs of MnC_n^- (n = 3-10) display very obvious odd-even alternation: the VDEs of MnC_n^- containing even number of C atoms are higher than those of their neighbors

TABLE I. Relative energies, VDEs, and ADEs of the low-lying isomers of MnC_n^- (n = 3-10) clusters obtained by theoretical calculations, as well as the experimental VDEs and ADEs estimated from their photoelectron spectra.[a]

					VDE (eV)		ADE (eV)							VDE (eV)		ADE (eV)	
	Isomer	State	Sym.	ΔE (eV)	Theo.	Expt.	Theo.	Expt.		Isomer	State	Sym.	ΔE (eV)	Theo.	Expt.	Theo.	Expt.
MnC_3^-	3A	$^3\Sigma$	$C_{\infty v}$	0.00	2.20	1.96	2.18	1.74	MnC_7^-	7A	$^5A_2$	C_{2v}	0.00	2.92	3.01	2.51	2.80
	3B	$^5\Sigma$	$C_{\infty v}$	0.004	2.32		2.18			7B	$^5A''$	C_s	0.16	3.33		3.13	
	3C	$^5B_1$	C_{2v}	0.078	2.03		1.90			7C	$^3\Sigma$	$C_{\infty v}$	0.25	3.12		3.09	
MnC_4^-	4A	$^7\Sigma$	$C_{\infty v}$	0.00	3.21	2.95	2.97	2.56	MnC_8^-	8A	$^7\Sigma$	$C_{\infty v}$	0.00	3.88	3.81	3.66	3.74
	4B	$^5\Sigma$	$C_{\infty v}$	0.12	2.96		2.86			8B	$^5\Sigma$	$C_{\infty v}$	0.13	3.69		3.53	
	4C	$^7A_1$	C_{2v}	0.29	2.81		2.41			8C	$^5A'$	C_s	0.79	2.77		2.15	
MnC_5^-	5A	$^5\Sigma$	$C_{\infty v}$	0.00	2.92	2.76	2.77		MnC_9^-	9A	$^5B_1$	C_{2v}	0.00	2.97	3.06	2.95	2.90
	5B	$^3\Sigma$	$C_{\infty v}$	0.06	2.74	2.47	2.71	2.30		9B	$^7B_1$	C_{2v}	0.03	3.00		2.92	
	5C	$^7B_1$	C_{2v}	0.45	2.47		2.41			9C	^5A	C_1	0.11	3.52		3.48	
MnC_6^-	6A	$^7\Sigma$	$C_{\infty v}$	0.00	3.66	3.64	3.38	3.54	MnC_{10}^-	10A	$^7A'$	C_s	0.00	3.99	3.97	3.85	3.91
	6B	$^5\Sigma$	$C_{\infty v}$	0.13	3.38		3.25			10B	$^5A'$	C_s	0.14	3.94		3.77	
	6C	$^7B_2$	C_{2v}	0.92	2.57		1.98			10C	$^5A'$	C_s	0.36	2.56		2.21	

[a]The uncertainties of the experimental values are ±0.08 eV.

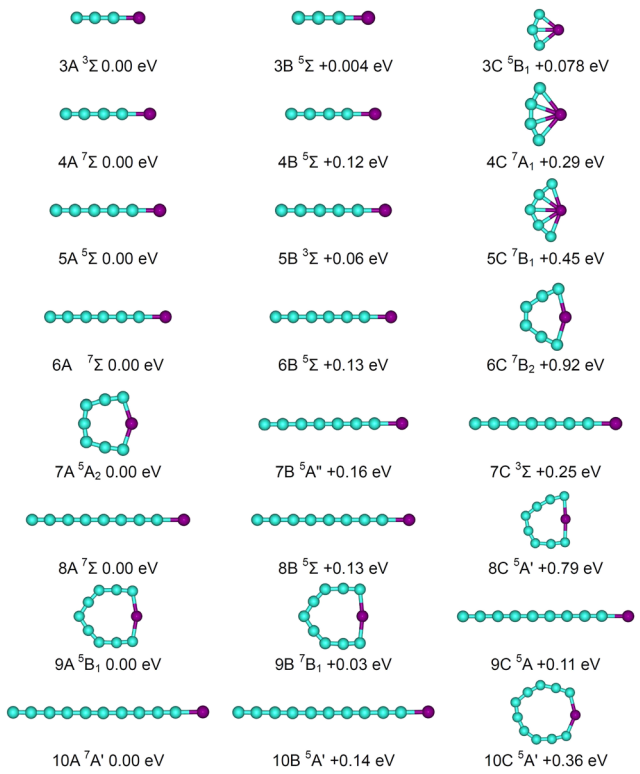

FIG. 2. Typical low-lying isomers of anionic MnC_n^- (n = 3-10) clusters. The cyan balls stand for the C atoms and the purple balls for the Mn atoms.

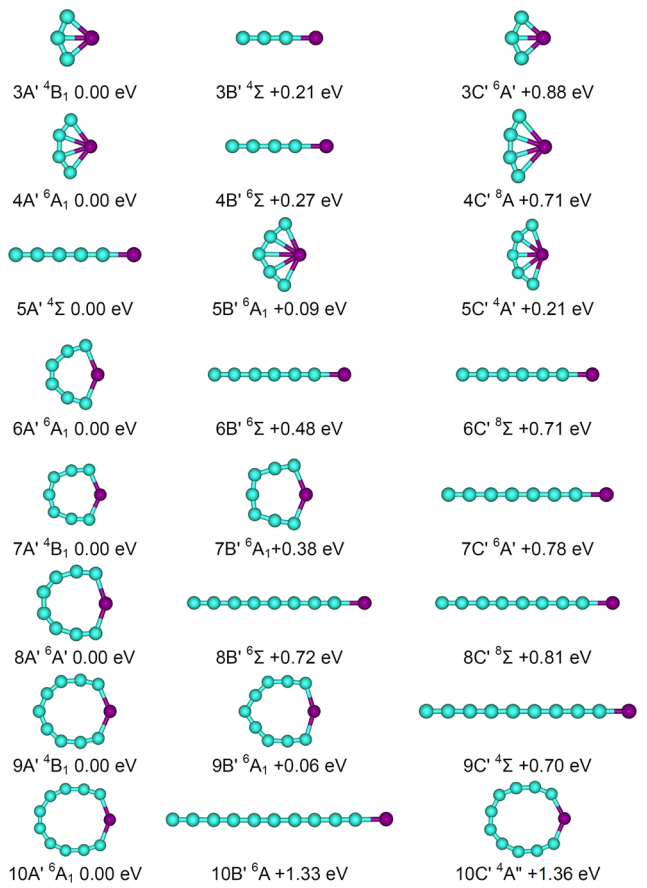

FIG. 3. Typical low-lying isomers of neutral MnC_n (n = 3-10) clusters. The cyan balls stand for the C atoms and the purple balls for the Mn atoms.

with odd number of C atoms. In addition, the VDEs increase with increasing number of carbon atoms in both odd and even series of MnC_n^-. As can be seen in Table I and Fig. 2, the spin multiplicities of the most stable isomers of MnC_n^- also show a parity effect: the n-odd clusters are in quintet (or triplet) states, whereas the n-even clusters are in septet states.

A. Structures of MnC_n^- (n = 3-10) anions

As can be seen in Fig. 2, the first two isomers of MnC_3^- are nearly degenerate in energy, with isomer 3B higher than isomer 3A by only 0.004 eV. They are linear structures in different electronic states with the Mn atom located at one end of the C_3 chain. They can be regarded as two electronic states of a linear structure. Here, we treat them as different isomers because they are different local minima on the energy surfaces. Isomer 3C is a fan-shaped structure with C_{2v} symmetry in a $^5B_1$ electronic state, in which the Mn atom interacts with the three carbon atoms. The energy of isomer 3C is higher than that of isomer 3A by 0.078 eV. The fanlike structure of MnC_3^- is in agreement with that reported by Wang and Li.[53] The theoretical VDEs of isomers 3A and 3C are 2.20 and 2.03 eV, respectively, both in reasonable agreement with the experimental value (1.96 eV). That of isomer 3B is calculated to be 2.32 eV, which may contribute to the tail of the first peak. The combination of the DOS spectra of three isomers is consistent with the experimental spectrum. To confirm the results of MnC_3^-, we also calculated the low-lying isomers of MnC_3^- at the MP2/6-311+G(3df) level.[63,64] The MP2 calculations also show that the three isomers are very close in energy with isomers 3C and 3A higher than 3B by only 0.01 and 0.11 eV, respectively. Thus, we suggest that isomers 3A, 3B, and 3C coexist in our experiments.

For MnC_4^-, isomers 4A and 4B are of $C_{\infty v}$ symmetry in different electronic states with the Mn atom located at one end of the C_4 chain. Isomer 4B is higher in energy than isomer 4A by 0.12 eV. Isomer 4C adopts a fan-shaped structure with the Mn atom connecting to the four carbon atoms. The theoretical VDEs of isomers 4A and 4B are 3.21 and 2.96 eV, respectively, both consistent with the experimental value (2.95 eV). Their simulated DOS spectra both fit the experimental spectrum very well. Thus, we suggest isomer 4A to be the most probable one detected in our experiments. Isomer 4B may have some contributions to the experimental spectrum. The existence of isomer 4C can be ruled out due to its high energy.

Isomers 5A and 5B are both linear structures with a terminal Mn atom. Isomer 5B is higher in energy than isomer 5A

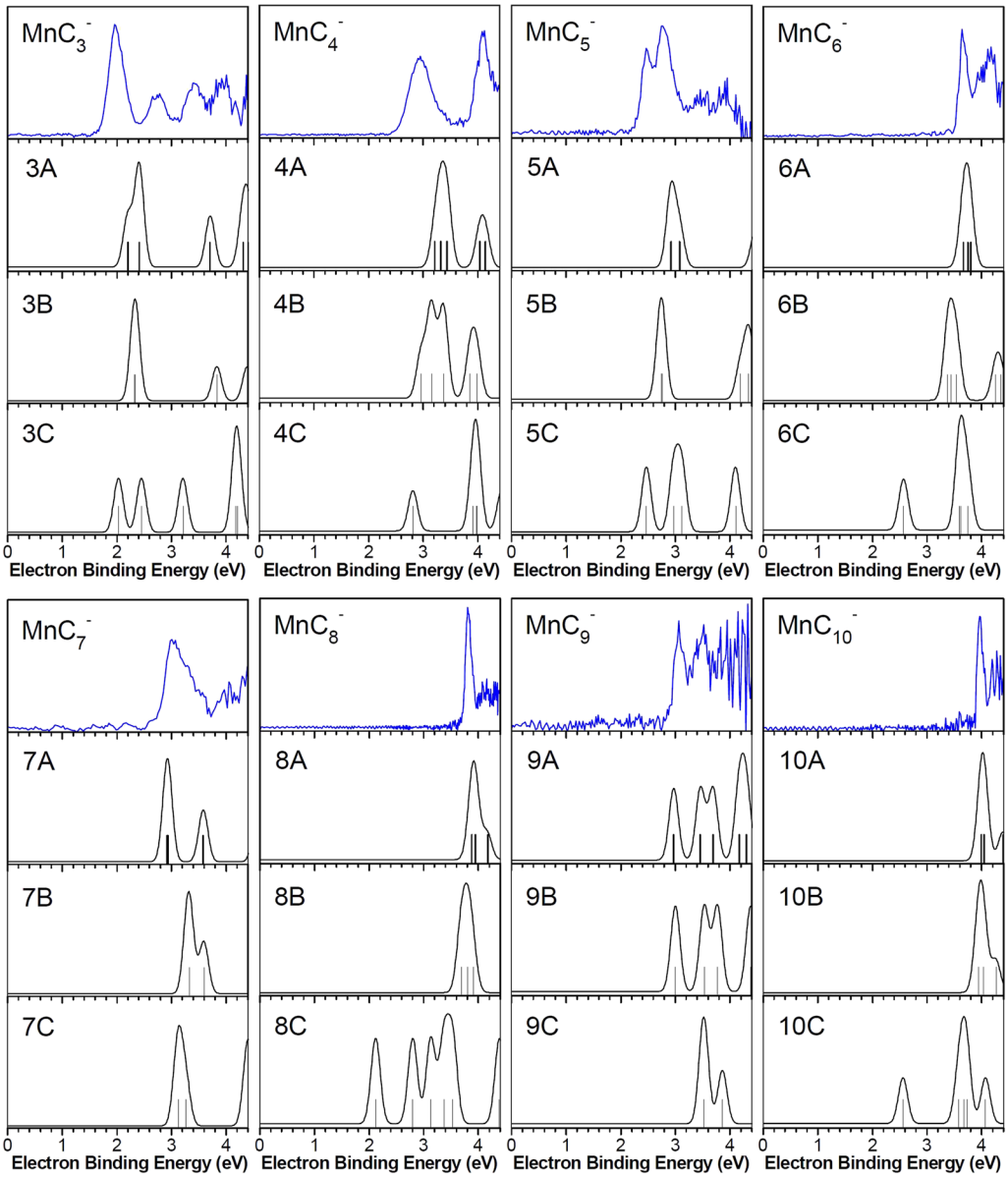

FIG. 4. Comparison of the experimental photoelectron spectra with the simulated DOS spectra of the low-lying isomers of MnC_n^- (n = 3-10) clusters. The simulations were conducted by fitting the distributions of the transition lines with unit-area Gaussian functions of 0.2 eV full width at half maximum. The vertical lines indicate the positions of theoretical spectral lines.

by only 0.06 eV. Isomer 5C is a fan-shaped structure with a carbon chain of C_5. Its energy is higher than that of isomer 5A by 0.45 eV. The calculated VDE of isomer 5A is 2.92 eV, which is in agreement with the second peak at 2.76 eV, and that of isomer 5B is 2.74 eV, which is in agreement with the first peak at 2.47 eV. As we can see in Fig. 4, the simulated DOS spectrum of isomer 5A may contribute to a part of the photoelectron features and that of isomer 5B agrees well with the other part in the experimental spectrum of MnC_5^-. The combination of the DOS spectra of isomers 5A and 5B can fit the experimental spectrum very well. Therefore, we suggest that isomers 5A and 5B coexist in our experiments.

For MnC_6^-, the first two isomers (6A and 6B) are both linear structures with the Mn atom located at one end of the C_6 chain. Isomer 6B is higher in energy than isomer 6A by 0.13 eV. Isomer 6C, a cyclic structure, is higher in energy than isomer 6A by 0.92 eV. The calculated VDE of isomer 6A is 3.66 eV, which is in excellent agreement with the experimental value

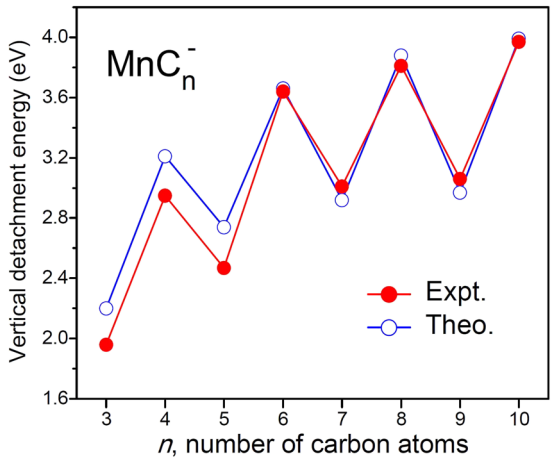

FIG. 5. Experimental and theoretical VDEs of MnC_n^- (n = 3-10) versus n, the number of carbon atoms.

(3.64 eV). The calculated VDE of isomer 6B is 3.38 eV, which is also in reasonable agreement with the experimental value. The simulated spectrum of isomer 6A can match the first peak very well, and that of isomer 6B is also in reasonable agreement with the experimental spectrum. The combination of the DOS spectra of isomers 6A and 6B can reproduce the experimental spectrum of MnC_6^-. Therefore, isomers 6A and 6B are suggested to be the most probable structures detected in our experiments.

As for MnC_7^-, the most stable isomer (7A) possesses a C_{2v} symmetric cyclic structure in a $^5A_2$ electronic state. The structure of isomer 7B is linear with a terminal Mn atom, whereas isomer 7C is a quasi-linear structure with C_s symmetry. Isomers 7B and 7C are higher in energy than isomer 7A by 0.16 and 0.25 eV, respectively. The calculated VDE of isomer 7A is 2.92 eV, which is in good agreement with the experimental value (3.01 eV). The theoretical VDE of isomer 7B (3.33 eV) is in line with the shoulder at 3.29 eV in the experimental spectrum. In Fig. 4, the simulated DOS spectrum of isomer 7A can fit most of the experimental features and that of isomer 7B is consistent with the shoulder in the experimental spectrum. The combined DOS spectra of isomers 7A and 7B are in good agreement with the experimental spectrum. Thus, isomers 7A and 7B may coexist in the cluster beam in our experiments.

Isomers 8A and 8B are linear structures in $^7\Sigma$ and $^5\Sigma$ electronic states, respectively. Isomer 8B is higher in energy than isomer 8A by 0.13 eV. The energy of isomer 8C is higher than that of isomer 8A by 0.79 eV. The theoretical VDE of isomer 8A (3.88 eV) is in excellent agreement with the experimental value (3.81 eV). In Fig. 4, the simulated spectrum of isomer 8A is in agreement with the experimental spectrum. The calculated VDE of isomer 8B (3.69 eV) is also consistent with the experimental value, and its DOS spectrum fits the first peak of the experimental spectrum well. Thus, we suggested isomer 8A to be the most likely structure for MnC_8^-. Isomer 8B may have some contributions to the first peak.

Isomers 9A and 9B are C_{2v} symmetric cyclic structures in $^5B_1$ and $^7B_1$ electronic states, respectively. Isomer 9C is a quasi-linear structure with a terminal Mn atom. Isomers 9B and 9C are higher in energy than isomer 9A by 0.03 and 0.11 eV, respectively. The calculated VDEs of isomers 9A and 9B are 2.97 and 3.00 eV, which is in excellent agreement with the experimental value (3.06 eV), and their DOS spectra can reproduce the peak positions and patterns of the photoelectron spectrum. Therefore, we suggested that isomers 9A and 9B coexist in our experiments. Isomer 9C may contribute to the signals in the range of 3.2–4.0 eV.

Isomers 10A and 10B are both quasi-linear structures with the Mn atom located at one end of the C_{10} chain. Isomer 10C is a cyclic structure in a $^5A'$ electronic state. The theoretical VDE of isomer 10A is 3.99 eV, which is in excellent agreement with the experimental value (3.97 eV). In Fig. 4, the simulated DOS spectrum of isomer 10A is in agreement with the experimental spectrum. Therefore, isomer 10A is suggested to be the most probable structure detected in our experiments. However, the existence of isomer 10B cannot be ruled out because its calculated VDE (3.94 eV) is consistent with the experimental value and its energy is slightly higher than that of isomer 10A by 0.14 eV. Isomer 10C can be excluded because its energy is higher than that of 10A by 0.36 eV.

B. Structures of MnC_n (n = 3-10) neutrals

The lowest-energy isomers of neutral MnC_3 (3A′) and MnC_4 (4A′) are fan-shaped structures in which the Mn atom interacts with all carbon atoms. The lowest-energy isomer of neutral MnC_5 (5A′) is a $C_{\infty v}$ symmetric linear structure with the Mn atom located at one end of the C_5 chain, similar to isomer 5A of MnC_5^-. The second isomer of MnC_5 (5B′) is a C_{2v} symmetric fanlike structure, which is higher in energy than isomer 5A′ by only 0.09 eV. The lowest-lying isomers of MnC_6, MnC_7, MnC_8, MnC_9, and MnC_{10} all have cyclic structures. The electronic states of the most stable isomers of MnC_n neutrals also show odd-even alternation: those containing odd number of carbon atoms are in quartet states, while those with even number of carbon atoms are in sextet states. Overall, the neutral MnC_n are more favorable to cyclic structures than their anionic counterparts.

C. ADCH charges and magnetic properties

We conducted the atomic dipole moment corrected Hirshfeld (ADCH) population analysis on the most stable isomers of the $MnC_n^{-/0}$ clusters. The excess spin density of the $MnC_n^{-/0}$ (n = 3-10) clusters is shown in Fig. 6. The total spin magnetic moments, atomic magnetic moments on the Mn atom, and charges on the Mn atom are summarized in Table II. From Fig. 6, it can be seen that the excess spin density mainly localizes on the Mn atom, while the excess spin density around the C atoms is relatively low. As can be seen from Table II, the negative charge is mainly localized on the C_n units for all anionic and neutral species, indicating that the electrons transfer from the Mn atom to the C_n units. That is reasonable because the electronegativity of a C atom (2.55) is much larger than that of a Mn atom (1.55).[65] The total spin magnetic

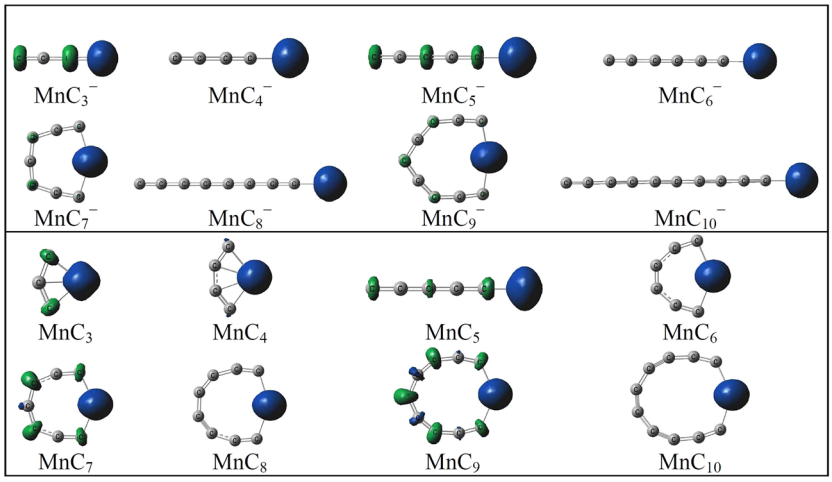

FIG. 6. Isosurfaces of the spin densities of the most stable isomers of $MnC_n^{-/0}$ (n = 3-10) clusters (isosurface value = 0.03 a.u.).

moments of MnC_n^- are 4 μ_B (2 μ_B for n = 3) when n is odd and 6 μ_B when n is even. The total spin magnetic moments of neutral MnC_n are 3 μ_B when n is odd and 5 μ_B when n is even. The local magnetic moments of the Mn atom in MnC_n^- anions range from 4.46 to 6.24 μ_B, and those in MnC_n neutrals are in the range of 3.89–4.97 μ_B; thus, the total spin magnetic moments are mainly contributed by the local magnetic moments on the Mn atom.

D. Evolution of the stability of $MnC_n^{-/0}$ with n

We investigate the relative stabilities of the $MnC_n^{-/0}$ clusters based on their binding energies per atom (E_b) and second-order energy differences (Δ_2E). The E_b and Δ_2E of the $MnC_n^{-/0}$ clusters are defined as follows:

$$E_b(MnC_n) = [E(Mn) + nE(C) - E(MnC_n)]/(n+1),$$

$$E_b(MnC_n^-) = [E(Mn) + (n-1)E(C) + E(C^-) - E(MnC_n^-)]/(n+1),$$

$$\Delta_2E(MnC_n^{-/0}) = E(MnC_{n-1}^{-/0}) + E(MnC_{n+1}^{-/0}) - 2E(MnCn^{-/0}),$$

TABLE II. Atomic dipole moment corrected Hirshfeld (ADCH) charges, local magnetic moments on Mn (μ_{Mn}), and total spin magnetic moments (μ_T) for the most stable isomers of $MnC_n^{-/0}$ (n = 3-10).

Anion	ADCH charge on Mn atom	μ_{Mn} (μ_B)	μ_T (μ_B)	Neutral	ADCH charge on Mn atom	μ_{Mn} (μ_B)	μ_T (μ_B)
MnC_3^-	−0.32	4.46	2	MnC_3	0.72	3.89	3
MnC_4^-	−0.14	6.13	6	MnC_4	0.74	4.57	5
MnC_5^-	−0.22	5.90	4	MnC_5	0.82	4.71	3
MnC_6^-	−0.06	6.18	6	MnC_6	0.74	4.84	5
MnC_7^-	0.45	4.67	4	MnC_7	0.70	4.54	3
MnC_8^-	0.00	6.20	6	MnC_8	0.77	4.81	5
MnC_9^-	0.50	4.90	4	MnC_9	0.84	4.86	3
MnC_{10}^-	0.04	6.24	6	MnC_{10}	0.87	4.97	5

where E is the energy of the corresponding atom or cluster. The E_b and Δ_2E values of the most stable isomers of $MnC_n^{-/0}$ versus n are plotted in Fig. 7. The E_b values of the anionic and neutral MnC_n clusters all increase monotonously with increasing number of carbon atoms. This suggests that the carbon-rich $MnC_n^{-/0}$ clusters are more stable than carbon-deficient ones. The E_b values of the anionic MnC_n clusters are larger than those of their corresponding neutral counterparts, indicating that an extra electron can strengthen the thermodynamic stabilities of these clusters. From Fig. 7, one can see that the Δ_2E values of the anionic and neutral MnC_n clusters both have strong odd-even oscillations with increasing number of carbon atoms, in which the Δ_2E values of n-even clusters are larger than those of adjacent n-odd clusters. This implies that the $MnC_n^{-/0}$ clusters with n-even have higher stabilities than their neighboring n-odd clusters, which is in good agreement with the change tendency of their VDEs.

To further evaluate the relative stabilities of the $MnC_n^{-/0}$ (n = 3-10) clusters, we also calculated the incremental binding energy (ΔE^I), which has been adopted to study the relative stabilities of C_nX (X = P, Sc, Ti, V, Co, and Fe).[35,41,66] ΔE^I is defined as the consecutive binding energy difference between adjacent $MnC_n^{-/0}$ and $MnC_{n-1}^{-/0}$ clusters, which can be obtained by the following formulas:

$$\Delta E^I(MnC_n^{-/0}) = \Delta E(MnC_n^{-/0}) - \Delta E\,(MnC_{n-1}^{-/0}),$$

$$\Delta E(MnC_n) = E(Mn) + nE(C) - E(MnC_n) = E_b(MnC_n) \times (n+1),$$

$$\Delta E(MnC_n^-) = E(Mn) + (n-1)E(C) + E(C^-) - E(MnC_n^-) = E_b(MnC_n^-) \times (n+1).$$

The incremental binding energies of the most stable isomers of $MnC_n^{-/0}$ versus the number of carbon atoms are shown in Fig. 7. The ΔE^I values of the anionic and neutral MnC_n clusters both display odd-even alternations with increasing number of carbon atoms although the parity effect is weak for MnC_{7-8}

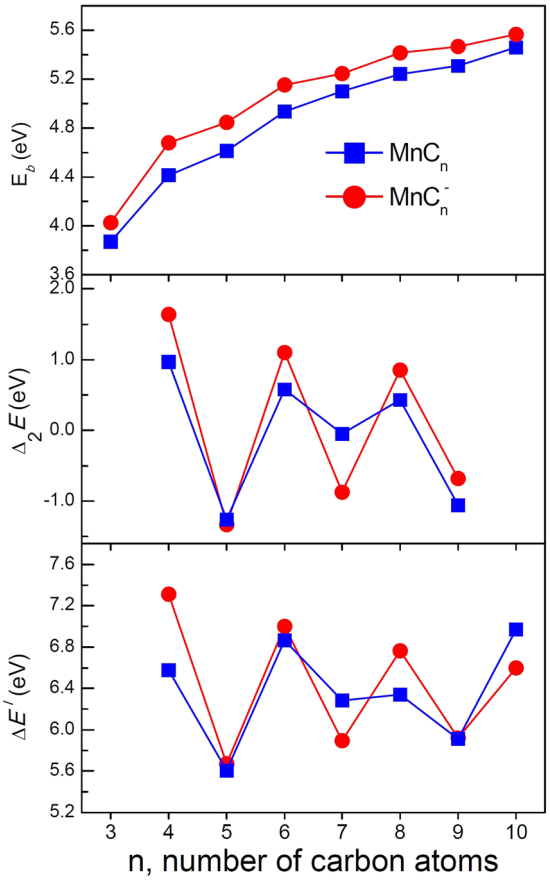

FIG. 7. Size-dependence of binding energies per atom (E_b), second-order energy difference ($\Delta_2 E$), and incremental binding energy (ΔE^I) for the most stable structures of $MnC_n^{-/0}$ (n = 3-10) clusters.

neutrals. The ΔE^I values with n-even clusters are larger than those with neighboring n-odd clusters. This indicates that the n-even $MnC_n^{-/0}$ clusters are more stable than the adjacent n-odd $MnC_n^{-/0}$ ones, as already ascertained above from the $\Delta_2 E$ considerations.

V. CONCLUSIONS

We investigated the structural and electronic properties of the $MnC_n^{-/0}$ (n = 3-10) clusters using size-selected anion photoelectron spectroscopy and density functional calculations. It is found that the vertical detachment energies of MnC_n^- display an obvious parity effect with increasing number of carbon atoms. The results show that MnC_3^- has three degenerate isomers with two linear structures in different electronic states and one fan-shaped structure. The MnC_n^- clusters, with n = 4-6, 8, and 10, all adopt linear structures with the terminal Mn atom. The most stable structures of MnC_7^- and MnC_9^- are both C_{2v} symmetric cyclic structures. For the neutral MnC_n clusters, the most stable structures are fan-shaped for MnC_3 and MnC_4, linear for MnC_5, and cyclic for $MnC_{6\text{-}10}$. The neutral MnC_n are more favorable to cyclic structures than their anionic counterparts. The ADCH population analysis indicates that the electrons transfer from the Mn atom to the C_n units and the magnetic moments mainly localize on the Mn atom. The odd-even alternations of the spin multiplicities and relative stabilities of $MnC_n^{-/0}$ are also observed.

SUPPLEMENTARY MATERIAL

See supplementary material for the relative energies and vertical detachment energies of the low-lying isomers of $MnC_{3\text{-}5}^-$ calculated from the B3LYP functional with the 6-311+G(d) and aug-cc-pVTZ basis sets, the Franck-Condon simulations of three isomers of MnC_3^-, and the Cartesian coordinates of low-lying isomers of MnC_n^- (n = 3-10) clusters.

ACKNOWLEDGMENTS

This work was supported by the National Natural Science Foundation of China (Grant No. 21773255), the Chinese Academy of Sciences (Grant No. QYZDB-SSW-SLH024), and the Beijing Municipal Science and Technology Commission (Grant No. Z181100004218004). The theoretical calculations were conducted on the China Scientific Computing Grid (ScGrid) of the Supercomputing Center, Computer Network Information Center of the Chinese Academy of Sciences.

REFERENCES

[1] B. C. Guo, K. P. Kerns, and A. W. Castleman, Jr., Science **255**, 1411 (1992).
[2] B. C. Guo, S. Wei, J. Purnell, S. Buzza, and A. W. Castleman, Jr., Science **256**, 515 (1992).
[3] J. S. Pilgrim and M. A. Duncan, J. Am. Chem. Soc. **115**, 6958 (1993).
[4] S. Li, H. B. Wu, and L. S. Wang, J. Am. Chem. Soc. **119**, 7417 (1997).
[5] Y. Chai, T. Guo, C. M. Jin, R. E. Haufler, L. P. F. Chibante, J. Fure, L. H. Wang, J. M. Alford, and R. E. Smalley, J. Phys. Chem. **95**, 7564 (1991).
[6] D. E. Clemmer, K. B. Shelimov, and M. F. Jarrold, Nature **367**, 718 (1994).
[7] Y. Zhong, X. H. Xia, F. Shi, J. Y. Zhan, J. P. Tu, and H. J. Fan, Adv. Sci. **3**, 1500286 (2016).
[8] M. Naguib, J. Come, B. Dyatkin, V. Presser, P.-L. Taberna, P. Simon, M. W. Barsoum, and Y. Gogotsi, Electrochem. Commun. **16**, 61 (2012).
[9] M. Naguib, M. Kurtoglu, V. Presser, J. Lu, J. J. Niu, M. Heon, L. Hultman, Y. Gogotsi, and M. W. Barsoum, Adv. Mater. **23**, 4248 (2011).
[10] F. Yang, X. Wang, D. Q. Zhang, J. Yang, D. Luo, Z. W. Xu, J. K. Wei, J. Q. Wang, Z. Xu, F. Peng, X. M. Li, R. M. Li, Y. L. Li, M. H. Li, X. D. Bai, F. Ding, and Y. Li, Nature **510**, 522 (2014).
[11] W. H. Chiang and R. M. Sankaran, Nat. Mater **8**, 882 (2009).
[12] D. S. Bethune, C. H. Klang, M. S. de Vries, G. Gorman, R. Savoy, J. Vazquez, and R. Beyers, Nature **363**, 605 (1993).
[13] P. Nikolaev, M. J. Bronikowski, R. K. Bradley, F. Rohmund, D. T. Colbert, K. A. Smith, and R. E. Smalley, Chem. Phys. Lett. **313**, 91 (1999).
[14] J. W. Fan and L. S. Wang, J. Phys. Chem. **98**, 11814 (1994).
[15] J. W. Fan, L. Lou, and L. S. Wang, J. Chem. Phys. **102**, 2701 (1995).
[16] X.-B. Wang, C.-F. Ding, and L.-S. Wang, J. Phys. Chem. A **101**, 7699 (1997).
[17] H. J. Zhai, L. S. Wang, P. Jena, G. L. Gutsev, and C. W. Bauschlicher, Jr., J. Chem. Phys. **120**, 8996 (2004).

[18]H.-J. Zhai, S.-R. Liu, X. Li, and L.-S. Wang, J. Chem. Phys. **115**, 5170 (2001).
[19]K. L. Knappenberger, Jr., P. A. Clayborne, J. U. Reveles, M. A. Sobhy, C. E. Jones, Jr., U. U. Gupta, S. N. Khanna, I. Iordanov, J. Sofo, and A. W. Castleman, Jr., ACS Nano **1**, 319 (2007).
[20]J. Y. Yuan, H. G. Xu, and W. J. Zheng, Phys. Chem. Chem. Phys. **16**, 5434 (2014).
[21]X. L. Xu, J. Y. Yuan, B. Yang, H. G. Xu, and W. J. Zheng, Chin. J. Chem. Phys. **30**, 717 (2017).
[22]J. Y. Yuan, P. Wang, G. L. Hou, G. Feng, W. J. Zhang, X. L. Xu, H. G. Xu, J. L. Yang, and W. J. Zheng, J. Phys. Chem. A **120**, 1520 (2016).
[23]Q. Zhang, L. C. Song, X. Lu, R. B. Huang, and L. S. Zheng, J. Mol. Struct. **967**, 153 (2010).
[24]P. Wang, W. J. Zhang, X. L. Xu, J. Y. Yuan, H. G. Xu, and W. J. Zheng, J. Chem. Phys. **146**, 194303 (2017).
[25]I. Leon, F. Ruiperez, J. M. Ugalde, and L. S. Wang, J. Chem. Phys. **149**, 144307 (2018).
[26]Z. Y. Li, L. R. Hu, Q. Y. Liu, C. G. Ning, H. Chen, S. G. He, and J. Yao, Chem. Eur. J. **21**, 17748 (2015).
[27]H. F. Li, Y. X. Zhao, Z. Yuan, Q. Y. Liu, Z. Y. Li, X. N. Li, C. G. Ning, and S. G. He, J. Phys. Chem. Lett. **8**, 605 (2017).
[28]H. F. Li, Z. Y. Li, Q. Y. Liu, X. N. Li, Y. X. Zhao, and S. G. He, J. Phys. Chem. Lett. **6**, 2287 (2015).
[29]P. Redondo, C. Barrientos, and A. Largo, J. Phys. Chem. A **109**, 8594 (2005).
[30]P. Redondo, C. Barrientos, and A. Largo, J. Phys. Chem. A **110**, 4057 (2006).
[31]L. Largo, Á. Cimas, P. Redondo, V. M. Rayón, and C. Barrientos, Int. J. Mass Spectrom. **266**, 50 (2007).
[32]P. Redondo, C. Barrientos, and A. Largo, J. Chem. Theory Comput. **2**, 885 (2006).
[33]P. Redondo, C. Barrientos, and A. Largo, Int. J. Mass Spectrom. **263**, 101 (2007).
[34]P. Redondo, C. Barrientos, and A. Largo, J. Mol. Struct.: THEOCHEM **769**, 225 (2006).
[35]P. Redondo, L. Largo, and C. Barrientos, Chem. Phys. **364**, 1 (2009).
[36]P. Redondo, C. Barrientos, and A. Largo, Int. J. Quantum Chem. **108**, 1684 (2008).
[37]C. Barrientos, P. Redondo, and A. Largo, Int. J. Mass Spectrom. **273**, 87 (2008).
[38]P. Redondo, C. Barrientos, and A. Largo, Int. J. Mass Spectrom. **272**, 187 (2008).
[39]C. Barrientos, P. Redondo, and A. Largo, J. Chem. Theory Comput. **3**, 657 (2007).
[40]L. Largo, A. Cimas, P. Redondo, V. M. Rayón, and C. Barrientos, Chem. Phys. **330**, 431 (2006).
[41]L. Largo, C. Barrientos, and P. Redondo, J. Chem. Phys. **130**, 134304 (2009).
[42]C. G. Li, J. Zhang, W. Q. Zhang, Y. N. Tang, B. Z. Ren, and Y. F. Hu, Sci. Rep. **7**, 17516 (2017).
[43]D. L. Strout and M. B. Hall, J. Phys. Chem. **100**, 18007 (1996).
[44]S.-J. Lu, Chem. Phys. Lett. **694**, 70 (2018).
[45]S.-J. Lu, Chem. Phys. Lett. **699**, 218 (2018).
[46]H. C. Urey, Phys. Rev. **88**, 248 (1952).
[47]N. I. Medvedeva, D. C. Van Aken, and J. E. Medvedeva, Comput. Mater. Sci. **96**, 159 (2015).
[48]J. J. He, P. B. Lyu, and P. Nachtigall, J. Mater. Chem. **4**, 11143 (2016).
[49]Y. G. Zhou and X. T. Zu, Electrochim. Acta **235**, 167 (2017).
[50]A. C. Borin and J. P. Gobbo, Chem. Phys. Lett. **417**, 334 (2006).
[51]G. L. Gutsev, L. Andrews, and C. W. Bauschlicher, Jr., Theor. Chem. Acc. **109**, 298 (2003).
[52]X. Li and L.-S. Wang, J. Chem. Phys. **111**, 8389 (1999).
[53]L.-S. Wang and X. Li, J. Chem. Phys. **112**, 3602 (2000).
[54]H. G. Xu, Z. G. Zhang, Y. Feng, J. Y. Yuan, Y. C. Zhao, and W. J. Zheng, Chem. Phys. Lett. **487**, 204 (2010).
[55]C. Lee, W. Yang, and R. G. Parr, Phys. Rev. B **37**, 785 (1988).
[56]A. D. Becke, J. Chem. Phys. **98**, 5648 (1993).
[57]M. J. Frisch, G. W. Trucks, H. B. Schlegel, G. E. Scuseria, M. A. Robb, J. R. Cheeseman, G. Scalmani, V. Barone, B. Mennucci, G. A. Petersson, H. Nakatsuji, M. Caricato, X. Li, H. P. Hratchian, A. F. Izmaylov, J. Bloino, G. Zheng, J. L. Sonnenberg, M. Hada, M. Ehara, K. Toyota, R. Fukuda, J. Hasegawa, M. Ishida, T. Nakajima, Y. Honda, O. Kitao, H. Nakai, T. Vreven, J. A. Montgomery, J. E. Peralta, F. Ogliaro, M. Bearpark, J. J. Heyd, E. Brothers, K. N. Kudin, V. N. Staroverov, T. Keith, R. Kobayashi, J. Normand, K. Raghavachari, A. Rendell, J. C. Burant, S. S. Iyengar, J. Tomasi, M. Cossi, N. Rega, J. M. Millam, M. Klene, J. E. Knox, J. B. Cross, V. Bakken, C. Adamo, J. Jaramillo, R. Gomperts, R. E. Stratmann, O. Yazyev, A. J. Austin, R. Cammi, C. Pomelli, J. W. Ochterski, R. L. Martin, K. Morokuma, V. G. Zakrzewski, G. A. Voth, P. Salvador, J. J. Dannenberg, S. Dapprich, A. D. Daniels, O. Farkas, J. B. Foresman, J. V. Ortiz, J. Cioslowski, and D. J. Fox, GAUSSIAN 09, Revision E. 01, Gaussian, Inc., Wallingford, CT, 2013.
[58]T. Lu and F. W. Chen, J. Theor. Comput. Chem. **11**, 163 (2012).
[59]T. Lu and F. W. Chen, J. Comput. Chem. **33**, 580 (2012).
[60]T. Lu and F. W. Chen, Acta Phys. Chim. Sin. **28**, 1 (2012).
[61]D. J. Tozer and N. C. Handy, J. Chem. Phys. **109**, 10180 (1998).
[62]J. Akola, M. Manninen, H. Häkkinen, U. Landman, X. Li, and L.-S. Wang, Phys. Rev. B: Condens. Matter Mater. Phys. **60**, R11297 (1999).
[63]M. Head-Gordon, J. A. Pople, and M. J. Frisch, Chem. Phys. Lett. **153**, 503 (1988).
[64]M. J. Frisch, M. Head-Gordon, and J. A. Pople, Chem. Phys. Lett. **166**, 275 (1990).
[65]L. Pauling, *The Nature of the Chemical Bond*, 3rd Ed. (Cornell University Press, Ithaca, New York, 1960).
[66]G. Pascoli and H. Lavendy, J. Phys. Chem. A **103**, 3518 (1999).